SIZE EFFECT ON SHEAR STRENGTH IN REINFORCED CONCRETE BEAMS WITH SHEAR REINFORCEMENT

N. Shirai and K. Moriizumi,
Department of Architecture, College of Science and Technology,
Nihon University, Tokyo, Japan
K. Ishii,
Kouzou soft, Co. Ltd., Tokyo, Japan

Abstract

The objective of the present paper is to investigate the size effect on shear strength in R/C beams. First, a four-point loading test on R/C beam specimens with a different size was carried out. Test results indicated that shear strengths depend on the size of specimens. Furthermore, an effect of variable parameters on shear strength was investigated. In the next place, tested R/C beam specimens were analyzed by the FE procedure, which incorporated a concept of the fracture mechanics, and the mechanism causing a size effect was clarified.

1 Introduction

In recent years, the scale of concrete structures is becoming larger and larger. However, this led to a new problem to be solved, which is known as "a size effect on strength". For instance, a size effect on flexural strength in plain concrete beams and on shear strength in R/C deep beams without shear reinforcement has been experimentally clarified, Shirai(1993) and Walraven(1993). Furthermore,

the former has been analytically verified by the FEM based on the fracture mechanics, Shirai(1993). On the other hand, as far as R/C beams with shear reinforcement failing in shear are concerned, no systematic experimental study has been conducted so far. In the present study, the four-point loading test on R/C beam specimens with shear reinforcement was conducted and a size effect and an effect of variable parameters on shear strength were investigated. Furthermore, the FE analysis was carried out on the tested R/C beam specimens and a mechanism causing a size effect was studied on the basis of dissipated fracture energy.

2 Test and results

2.1 Test program

Variable parameters selected are as follows: (1)size of specimens($b \times D$; b: width, D: depth), (2)spacing of shear reinforcement(S), (3)shear span ratio(a/D; a: shear span length), (4)maximum size of aggregate(d_a) and (5)design yield strength of shear reinforcement (f_{sy}). Three series of specimens; that is, L-series(4 specimens) with actual size, M-series(3 specimens) with 1/2 scale and S-series(2 specimens) with 1/4 scale, were prepared. Fig. 1 shows the dimension
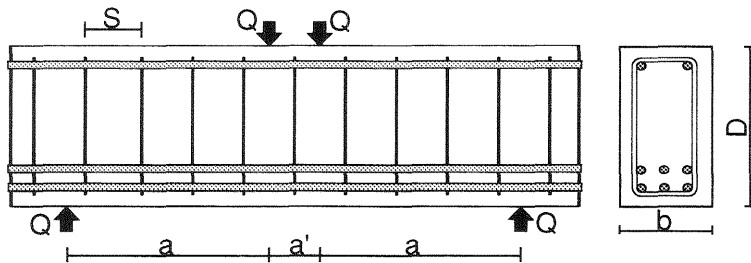

Fig. 1 Detail of specimens

Table 1 Structural details of specimens

Series	Size(mm)				Shear Reinforcemnent				Main bar	Concrete
	b	D	a	a'	Type	S(mm)	Ps(%)	fsy(MPa)	Type	da(mm)
L-PROT					2-D13*	240	0.35	294		13
-S025	300	600	600	200	2-D6	60	0.35	294	6-D25	13
- da					2-D13	240	0.35	294		25
- RT					2-D6	140	0.15	686		13
M-PROT			300		2-D6	120				
-S025	150	300	300	200	2-D3	27	0.35	294	6-D13	13
-SPAN			600		2-D6	120				
S-PROT	75	150	150	150	2-D3	53	0.35	294	6-D6	13
-SPAN			300							

* 2-D13 indicates two deformed bars with nominal diameter of 13 mm.

and bar arrangement of typical specimen. The structural details of specimens are listed in Table 1. B-L-PROT, B-M-PROT and B-S-PROT are the reference specimens and are referred to as the "prototype". Material properties for concrete and reinforcement used are listed in Tables 2 and 3, respectively. Loading method adopted is the four-point loading of simple beam type. Load was applied by means of the Universal Testing Machine. Displacements were measured using four displacement transducers installed on the front and rear sides of specimen. That is, the vertical displacements at the loading points relative to the supporting points were measured. Strains in main and shear reinforcement were also measured using the strain gauges.

2.2 Test results

Maximum strengths($\tau_u = Q_u/bj$) and fracture modes are listed in Table 4. Where Q_u means the applied force at the peak, j equals to $7d/8$ and d is the effective depth of beams. Note that the predicted values of τ_u by Bažant's shear strength formula, Bažant et al.(1989), and the FE procedure to be stated in the next section are also listed in the same table. Figs. 2(a) and (b) show the observed crack patterns at $\tau_A(= Q/bj) = 1.96\,\text{MPa}$ and at the peak, respectively. Where Q means the applied force. τ_u varys depending on a

Table 2 Material properties of concrete

da(mm)	σ_B^{*}(MPa)	Ec^{**}(GPa)
13	28.8	24.5
25	29.3	27.5

* Compressive strength
** Young's modulus

Table 3 Material properties of reinforcemenet

Type	σ_{sy}^{*}(MPa)	Ec^{**}(GPa)
D25	381	179
D13	376	193
D6	412	177
D6	913	212
D3	370	173

* Yield strength ** Young's modulus

Table 4 Maximum strengths and fracture modes

Series	Measured value	Bažant's formula		F.E.M		Fracture mode
	(1) τ u(MPa)	(2) τ u(MPa)	(1)/(2)	(3) τ u(MPa)	(1)/(3)	
L-PROT	5.11	5.50	0.93	5.08	1.01	Shear
-S025	6.15	5.52	1.11	6.09	1.01	
- da	5.85	5.68	1.03	5.59	1.05	
- RT	6.06	5.56	1.10	6.30	0.96	
M-PROT	5.59	6.46	0.87	6.08	0.92	Shear
-S025	6.05	6.33	0.96	6.40	0.95	Shear
-SPAN	3.49	—	—	—	—	Flexure
S-PROT	6.88	7.00	0.98	6.51	1.06	Shear
-SPAN	3.76	3.27	1.15	—	—	

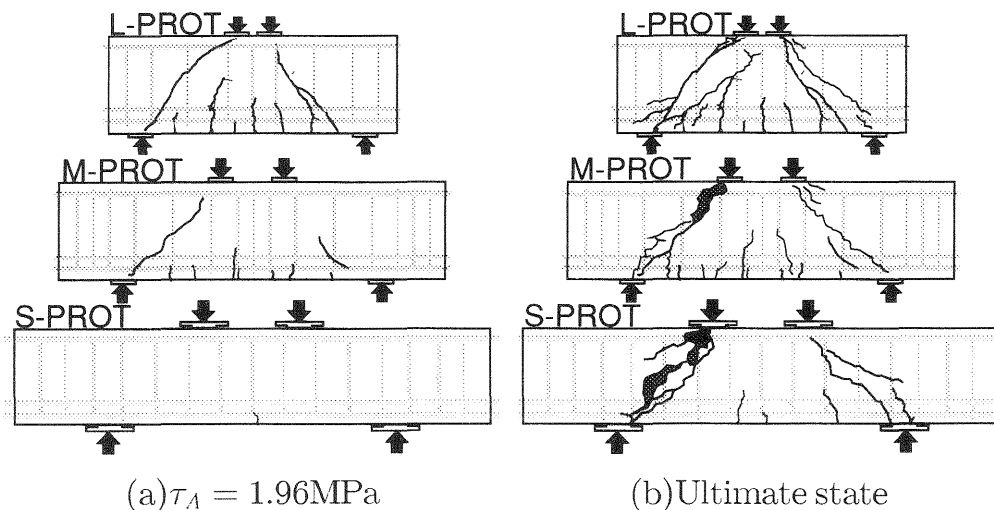(a)$\tau_A = 1.96$MPa   (b)Ultimate state

Fig. 2 Observed crack patterns

size of specimens and other variable parameters. On the other hand, fracture progression of the specimens, except for B-M-SPAN failing in flexure, was almost similar to each other. However, Fig. 2(a) indicates that a rate of crack propagation is different depending on a size of specimens. In the next place, an effect of D, S and d_a on shear strength shall be investigated. τ_U are plotted against D in Fig. 3. The predicted values by Bažant's formula and the FE procedure are also plotted in the figure. The shear strength decreases with an increase in beam's size even for R/C beams with shear reinforcement. Bažant's formula, which considers a size of beam and aggregate, and the FE procedure, can predict the observed tendency fairly well. Fig. 4 shows the comparison of τ_U–S relations for the specimens with the same P_s but different S. The shear strength increases when S value becomes smaller in keeping P_s identical. However, it does not hold all the time. Because almost no difference between the shear strengths of B-L-S025 ($D = 600$ mm, $S = 60$ mm) and B-M-S025 ($D = 300$ mm, $S = 27$ mm) is observed. This indicates that a size effect on shear strength disappears when P_s or S exceeds a certain limit. It is seen from Table 4 that the shear strength of B-L-da with larger aggregate size($d_a = 25$ mm) is slightly higher than that of B-L-PROT with smaller aggregate size ($d_a = 13$ mm). Note that D, P_s and S were kept constant for both specimens. This may be due to the aggregate interlocking action along rough crack surfaces. The observed shear crack surface of B-L-da was meandering larger than that of B-L-PROT. This roughness of crack surfaces led to an increase of aggregate interlocking action causing an incease of shear resistance.
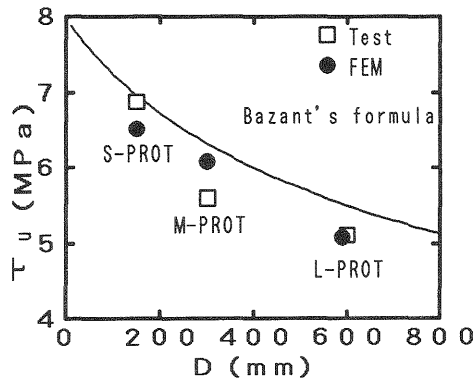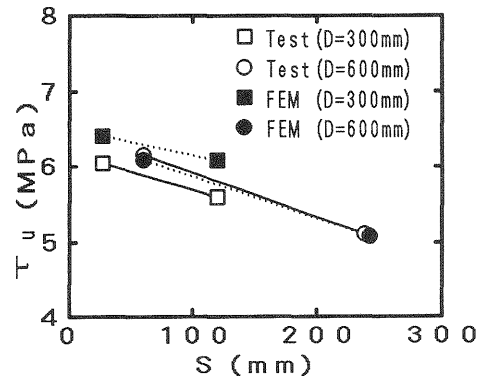
Fig. 3　τ_u–D relation

Fig. 4　τ_u–S relation

3 Analytical model and numerical results

3.1 Analytical model

In order to simulate fracture behaviors of the R/C beams, it is a keypoint how to model cracking and compressive fracture behaviors of concrete. In this study, shear crack dominating the fracture mode shall be modelled by the fictitious crack model, Hillerborg(1985), and other cracks shall be modelled by the microplane model (hereinafter, refers to as MP–model). The former behavior of cracks is expressed by the linkage element, which has two independent springs normal and parallel to crack surface (K_n, K_t), and the latter behavior of concrete including cracks is expressed by the constant triangular element. The reinforcement is modelled by the truss element and a bilinear stress–strain relationship is assumed. Bond–slip behavior between main bars and concrete is modelled by the linkage element and the bond stress–slip relationship is assumed. The earliest version of MP–model, Bažant et al.(1985), is adopted for its simplicity. The use of MP–model is mainly intended to express compressive fracture behavior of concrete. However, the original model can not express such behavior since the compressive softening after the peak is not assumed in the normal microstress(s_n)–microstrain(e_n) relation on weak planes in concrete. Thus, the s_n–e_n relation is modified to consider the compressive softening. There exists a fracture process zone in front of a crack tip where microcracks are generated and developed. It is considered that Mode I and Mode II are coexisting in this zone. Mechanical property of Mode I has been clarified through the direct tension or flexural test on plain concrete and is known as the tension softening in which tensile stress (σ) decreases with an increase in opening displacement (δ_n). The area under this σ–δ_n curve is referred to as the fracture energy of Mode I (G_{FI}) and

is regarded as the material property. On the other hand, mechanical property of Mode II has not been experimentally clarified but it is modelled as the shear softening similar to the tension softening. Thus, the area under the shear stress (τ)– slip displacement (δ_s) curve; that is, the fracture energy of Mode II (G_{FII}), is also regarded as the material property. Furthermore, the aggregate interlocking against slip displacement (δ_s) along crack surfaces activates in the back zone of crack tip. This shear transfer is also modelled as the shear stress (τ_a) –slip displacement (δ_s) relation. It is assumed that σ–δ_n and τ–δ_s relations have the same configuration and represented by the bilinear model as shown in Fig. 5. With reference to the past test result, Fenwick et al.(1968), the τ_a–δ_s relation is modelled by a bilinear curve as shown in Fig. 5(c) under a constant opening displacement $(\delta_n = const.)$. Note that the initial stiffness (K_{ta}) and the yield shear stress (τ_{ay}) are given in terms of δ_n. The properties described in the above are represented by the linkage element shown in Fig. 6. The σ–δ_n relation is expressed by the spring K_n and the τ–δ_s and τ_a–δ_s relations are expressed by the spring K_t which is derived by coupling the respective springs K_{tF} and K_{ta} in parallel. Note that an initiation of crack follows the Mohr–Coulomb fracture criterion with tension cut-off.
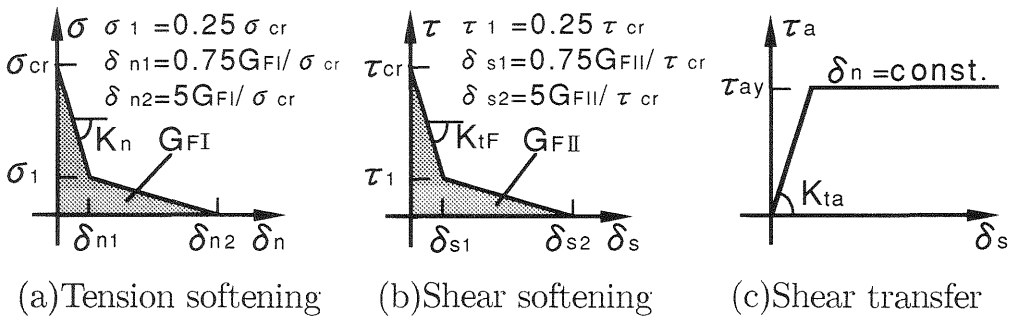

(a)Tension softening   (b)Shear softening   (c)Shear transfer

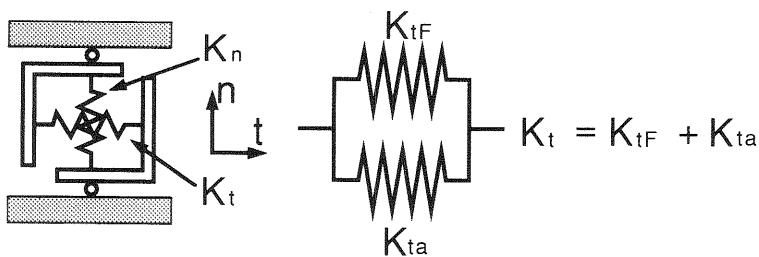Fig. 5 σ–δ_n, τ–δ_s and τ_a–δ_s relations

Fig. 6   Linkage element

3.2 Numerical results and discussion

Fig. 7 shows the mesh devision of B-M-PROT. The position of discrete cracks was so allocated that it simulates the observed major shear cracks. The fracture energy of Mode I (G_{FI}) was assumed to be $G_{FI} = 0.2\,\text{Nmm/mm}^2$ to consider the confining effect of shear reinforcement. Parametric study was conducted to determine the fracture energy of Mode II (G_{FII}) by changing α value from 0.5 to 2.0, provided that $G_{FII} = \alpha\,G_{FI}$. $\alpha = 0.5$, which gives reasonable predictions, was adopted. Fig. 8 compares the calculated and observed τ_A–δ_c/a curves for the prototype specimens. Their agreements are reasonably good. The analytical results in Fig. 3 also indicate that the size effect on shear strength exists even for the R/C beams with shear reinforcement. Finally, a mechanism causing a size effect is studied by evaluating dissipated energy qualitatively. It is assumed that energies dissipated along the shear crack line can be defined as follows.

$$U_c = U_{G_{FI}} + U_{G_{FII}} + U_{G_a} = \sum A_i \left(\int \sigma\, d\delta_n + \int \tau\, d\delta_s + \int \tau_a\, d\delta_s \right) \quad (1)$$

$$\bar{U}_c = U_c/A_c,\ \bar{U}_{G_{FI}} = U_{G_{FI}}/A_c,\ \bar{U}_{G_{FII}} = U_{G_{FII}}/A_c,\ \bar{U}_{G_a} = U_{G_a}/A_c \quad (2)$$

where U_c is the dissipated total energy, $U_{G_{FI}}$, $U_{G_{FII}}$ and U_{G_a} the dissipated total energies corresponding to the tension softening, shear softening and aggregate interlocking, $\bar{U}_c$ the dissipated total energy per unit area, $\bar{U}_{G_{FI}}$, $\bar{U}_{G_{FII}}$ and $\bar{U}_{G_a}$ the dissipated total energies per unit area corresponding to the tension softening, shear softening and aggregate interlocking, A_i the area covering the i-th linkage element and A_c the area of shear crack surface. Fig. 9 shows the relationship between the dissipated total energy per unit area ($\bar{U}_c$) and the depth of beams (D). Amount of $\bar{U}_c$ for B-M-PROT is the
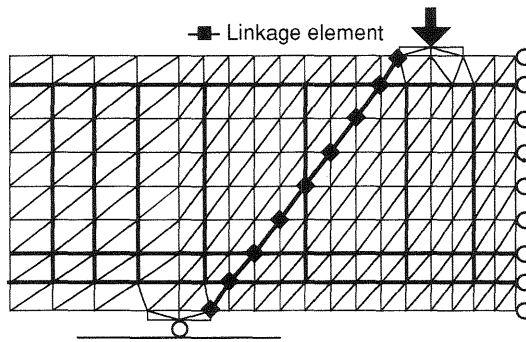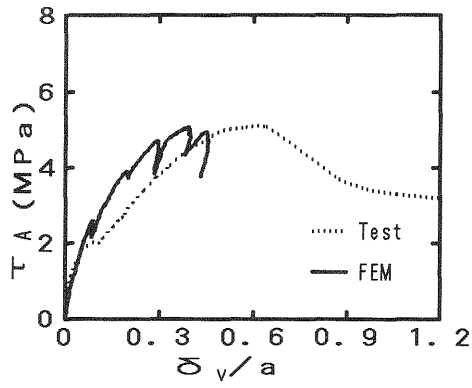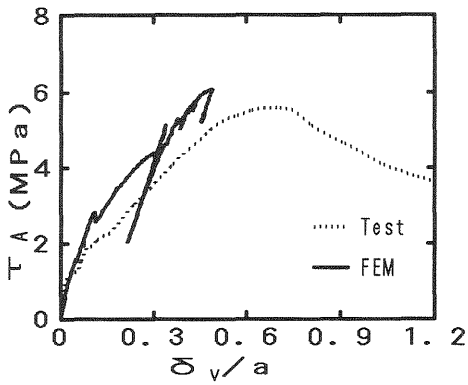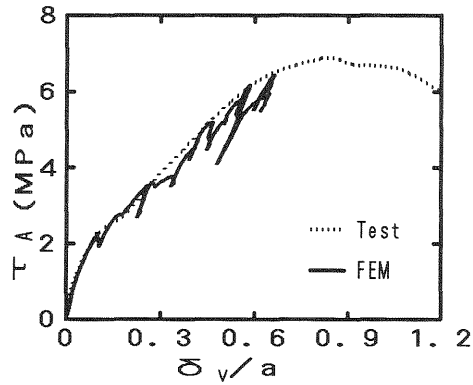

Fig. 7   Finite element descretization

(a)L-PROT

(b)M-PROT

(c)S-PROT
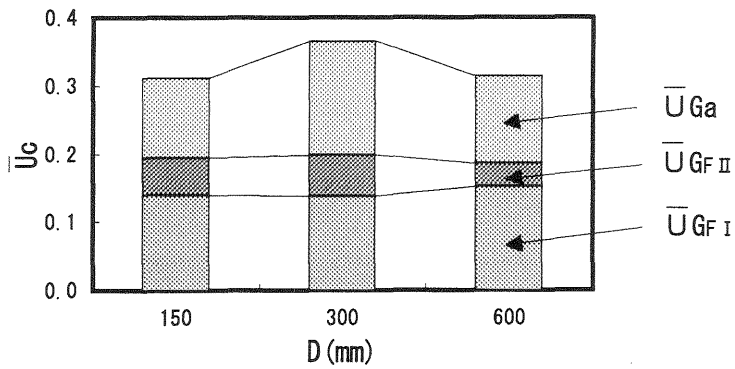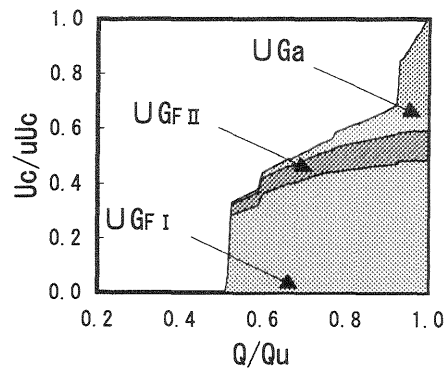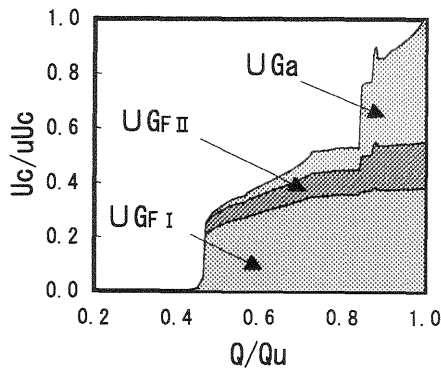
Fig. 8 τ_A–δ_v/a curves
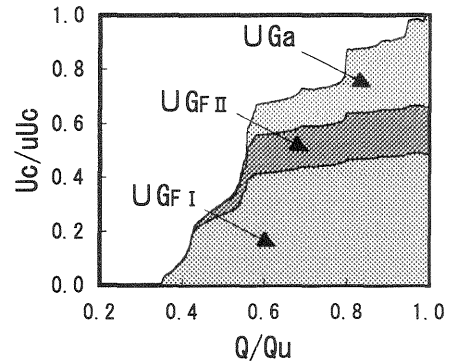

Fig. 9 Dissipated total energy per unit area

most, then B-L-PROT and that for B-S-PROT is the least. Fig. 10 shows the transition of the ratio $(U_c/{_u}U_c)$ of dissipated total energies of each component $(U_c = U_{G_{FI}} + U_{G_{FII}} + U_{G_a})$ to the dissipated total energy $({_u}U_c)$ up to the peak. It is seen that the dissipation process of component energies is different depending on a size of specimens. In the case of B-L-PROT, all $U_{G_{FI}}$ is spent in a relatively earlier stage than the other specimens and thus it is said that the fracture of Mode I was dominant. In the case of B-M-PROT, although the dissipation process of component energies is similar to that of B-L-PROT, the total amount of U_{G_a} is larger than that of B-L-PROT and thus a contribution of aggregate interlocking is significant. In the case of B-S-PROT, U_{G_a} starts to dissipate earlier than the others. In addition, the total amount of $\bar{U}_{G_{FI}}$ is smaller than that of B-L-PROT. It can be said from the said facts that the shear reinforcement still has a room to share stresses and this led to higher shear strength than the others.

(a)L-PROT

(b)M-PROT

(c)S-PROT

fig.10 $U_c/{_u}U_c$–Q/Q_u relations

4 Conclusions

The size effect in R/C beams was studied and the following conclusions were obtained. First, it was experimentally clarified and analytically verified that a size effect on shear strength exists even for R/C beams with shear reinforcement. Secondly, it is considered that the size of aggregate and spacing of shear reinforcement are major sources causing a size effect on shear strength. Finally, it is possible to understand a mechanism causing a size effect by examining total amount of dissipated energy and dissipation process of energy along the shear crack surfaces.

5 Acknowledgement

6 References

Bažant, Z.P. and Oh, B.H.(1985) Microplane model for progressive fracture of concrete and rock. **Journal of Structural Engineering**, ASCE, 111(4), 559–582.

Bažant, Z.P. and Sun, H.H.(1987) Size effect in diagonal shear failure: influence of aggregate size and stirrups. **ACI Materials Journal**, 259–272.

Fenwick, R.C. and Paulay, T.(1968) Mechanisms of shear resistance of concrete beams. **Proc. of the ASCE**, Vol.94, No.ST10, 2325–2350.

Hillerborg, A.(1985) The theoretical basis of a method to determine the fracture energy G_F of concrete. **Materials and Structures**, 18(106), 25–30.

Shirai, N.(1993) JCI Round Robin analysis of size effect in concrete structures, in **Size Effect in Concrete Structures** (eds H. Mihashi, H. Okamura and Z.P. Bažant), Proc. of the Japan Concrete Institute International Workshop, 295–322.

Walraven, J.C.(1993) Size effects : their nature and their recognition in building codes, in **Size Effect in Concrete Structures** (eds H. Mihashi, H. Okamura and Z.P. Bažant), Proc. of the Japan Concrete Institute International Workshop, 375–394.